Pergamon

Int. J. Heat Mass Transfer. Vol. 41, No. 2, pp. 465–474, 1998

Printed in Great Britain
0017–9310/98 $19.00+0.00

PII: S0017–9310(97)00131–2

Experimental studies and numerical simulation of evaporative cooling of air with a water spray—II. Horizontal counter flow

S. S. KACHHWAHA,† P. L. DHAR and S. R. KALE‡

Mechanical Engineering Department, Indian Institute of Technology, Hauz Khas, New Delhi-110016, India

(*Received* 13 *January* 1997)

Abstract—Hollow cone water sprays are used in many humidifying, cooling and scrubbing applications. In a companion paper by Kachhwaha *et al.* Experimental studies and numerical simulation of evaporative cooling of air with a water spray: Part I—horizontal parallel flow. *International Journal of Heat and Mass Transfer*, 1996a (submitted), a detailed study of hollow cone water sprays in horizontal parallel flow has been given. In this paper the studies have been extended to a horizontal counterflow configuration where reversal of the direction of motion of some drops is considered. These set of equations are space marched numerically and the solution is obtained in an iterative manner. The water spray nozzle was located at the wind tunnel exit face, facing upstream, for obtaining experimental data for this configuration. Model predictions of air condition change agree well with experimental data. © 1997 Elsevier Science Ltd.

1. INTRODUCTION

Water spray based evaporative cooling is used in many applications and is an especially attractive alternative during hot dry summers because of its low energy requirement. One of the various configurations which are employed, namely, horizontal parallel flow, was studied in detail and reported by Kachhwaha *et al.* [1] in a companion paper. In this paper, the model and experiments have been extended to another configuration, namely, horizontal counter flow.

The counter flow configuration is considerably more complex because some drops undergo reversal of their stream-wise velocity component. Thus, during the initial portion of their travel, counter flow condition exists, but during the later part it is a parallel flow configuration. An additional complexity is introduced by the fact that in the space marching scheme only one boundary condition is known, i.e. air condition. Therefore, the mathematics has to be adopted to make it a pseudo-parallel flow system so that explicit marching can be carried out. This simplification necessitates guessing the outlet condition and then computing the inlet air condition. Numerically, this process is performed by an iterative scheme which makes the codes more complex.

The literature review given in Kachhwaha *et al.* [1] gives an overall description of literature relevant to the present studies. Like horizontal parallel flow there is very little reported work on heat and mass transfer in horizontal counter flow configuration of a spray in an air stream. Most work on spray characterization has been carried out in quiescent atmosphere and, therefore, the influence of surrounding gas phase flow on spray formation is not considered. Hence, in the present research also, the spray formation has been taken in still air and the results obtained were used as initial conditions for the heat and mass transfer modelling of both configurations. The detailed description of the counter flow model is given below.

2. HEAT AND MASS TRANSFER MODEL

The control volume shown in Fig. 1 has air flow from left to right with spray directed upstream from the exit face centre. Some drops, such as *A* in Fig. 1, do not experience reversal of trajectory, whereas others penetrate the wind tunnel for some distance (*B*) and then reverse their trajectory (*C*). Thus, all drops start moving from right to left and after some distance, some undergo reversal of trajectories and move from left to right. Conservation equations for back flowing drops are similar to those for the forward moving drops, except that x-direction drop velocity varies between zero to air velocity with negative magnitude.

The choice of x–y coordinates for this configuration is shown in Fig. 1. The origin is at the nozzle spray sheet break-up with x-direction increasing inwards into the duct. The y-axis is vertically downwards as shown and it is the same as in the parallel flow configuration. The mass, momentum and energy con-

† Present address: Department of Mechanical Engineering, Engineering College, Kota-324010, India.

‡ Author to whom correspondence should be addressed.

NOMENCLATURE

A	cross-section area of the test section
A_s	surface area of drop
C_D	coefficient of drag
$C_{p,av}$	average specific heat of air
C_{pd}	specific heat of drop
D	drop diameter
DBT	dry bulb temperature
g	constant for gravity
h	heat transfer coefficient
h_a	enthalpy of air
h_{fg}	enthalpy of evaporation
$h_{fg,wall}$	enthalpy of evaporation of duct wall
$h_{fg,0}$	enthalpy of evaporation of 0°C
h_m	mass transfer coefficient
$h_{m,wall}$	mass transfer coefficient of inner duct wall
h_{wall}	heat transfer coefficient of inner duct wall
m	mass flow rate of water vapour
N	number of drops per second
n	number of drops per second per unit cross-section area of duct
p	periphery of duct
T_a	air temperature
T_d	drop temperature
T_{wall}	temperature of duct wall surface
t	time
U	drop velocity
U_x	drop velocity in x-direction
U_y	drop velocity in y-direction
u	air velocity inside the duct
W	relative velocity of drop w.r.t. air
X	mass fraction of water vapour
X_s	mass fraction of water vapour at the drop surface
X_{wall}	mass fraction of water vapour at the surface of duct wall
x	positive direction along the duct.

Greek symbols

ρ_a	density of air
ρ_l	density of water.

Subscripts

a	air
av	average condition
b	back flow
d	drop, drag
fg	evaporation
i	general designation, drop volume space
j	backward flowing category
l	liquid condition
m	mass transfer condition
s	surface, saturation condition
v	vapour
vs	saturation condition of vapour
w	water
wall	duct wall condition
x	coordinate
y	coordinate
0	zero Celsius.

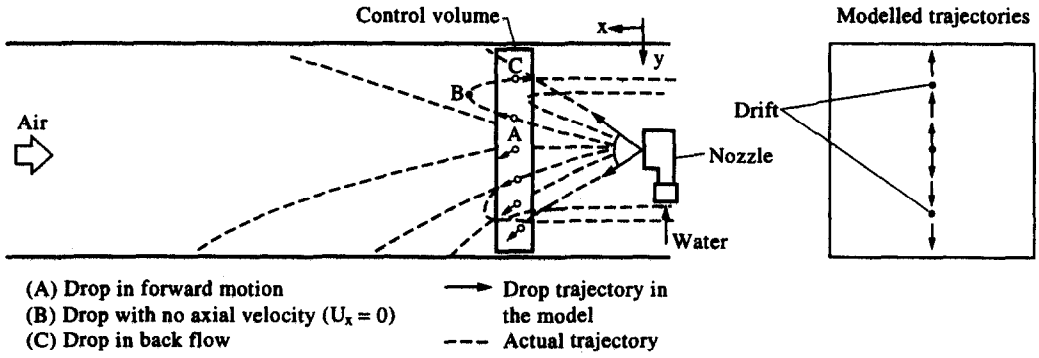

Fig. 1. System for flow modelling in horizontal counter flow configuration.

servation equations for this model are described below.

2.1. *Conservation of mass*

Due to redefinition of x-direction, the conservation equation for water vapour is derived and expressed in terms of the mass fraction of water vapour in air, as:

$$\frac{dX}{dx} = -\frac{1}{A\rho_a}\left[\frac{dm_v}{dx} + \frac{dm_{wall}}{dx}\right] - \frac{X}{u}\frac{du}{dx} - \frac{X}{\rho_a}\frac{d\rho_a}{dx} \quad (1)$$

Similarly conservation of mass for air can be written as:

$$\rho_a(1-X)uA = \text{constant}. \quad (2)$$

The conservation equations for drop motion need to be written separately for the forward moving and backward moving drops.

2.1.1. *Forward moving drops.* This equation is same as that for parallel flow, as the x-axis has been redefined to be coincident with the spray direction. For polydisperse drops:

$$\frac{dD_i}{dx} = \frac{-2h_{m,i}\rho_a(X_{s,i}-X)}{\rho_l U_{x,i}}. \quad (3a)$$

2.1.2. *Backward moving drops.* The mass conservation is similar to equation (3a) and for polydisperse back flowing drops it can be written as:

$$\frac{dD_{b,j}}{dx} = \frac{-2h_{mb,j}\rho_a(X_{sb,j}-X)}{\rho_l U_{xb,j}}. \quad (3b)$$

The term dm_v/dx in equation (1) is equal to the sum of the contributions due to forward and backward moving drop categories.

$$\frac{dm_v}{dx} = \left[\sum_i n_i \frac{dM_{d,i}}{dx}\right] + \left[\sum_j n_{b,j}\frac{dM_{db,j}}{dx}\right]. \quad (4)$$

2.2. *Conservation of momentum for air*

As discussed in Kachhwaha [2], there is negligible momentum transfer from spray to air and therefore air velocity remains practically unaltered. The momentum equations for forward and backward moving polydisperse drops are as follows.

2.2.1. *Forward moving drops.* The x- and y-momentum equations for forward moving drops are similar to the equations used for parallel flow, except for the effect of relative directions of motion of air and drops.

$$\frac{dU_{x,i}}{dx} = -\frac{3}{4}\frac{C_{D,i}\rho_a W_i(U_{x,i}+u)}{U_{x,i}\rho_l D_i} - \frac{3U_{x,i}}{D_i}\frac{dD_i}{dx} \quad (5)$$

$$\frac{dU_{y,i}}{dx} = \frac{g(\rho_l-\rho_a)}{\rho_l U_{x,i}} - \frac{3}{4}\frac{C_{D,i}\rho_a W_i U_{y,i}}{\rho_l D_i U_{x,i}} - \frac{3U_{y,i}}{D_i}\frac{dD_i}{dx}. \quad (6)$$

In these equations, relative velocity, W_i is defined as

$$W_i = [(U_{x,i}+u)^2 + U_{y,i}^2]^{1/2}. \quad (7)$$

2.2.2. *Backward moving drops.* The x- and y-momentum equations are similar to equations (5) and (6) for forward moving drops, but with air velocity subtracted from x-component of drop velocity. Drop trajectory equations for forward and backward flowing drops are similar to those for parallel flow configuration [1].

2.3. *Conservation of energy*

The conservation of energy equation for air is similar to the equation in parallel flow with an additional term due to contribution from back moving drops. The equation can be written as follows:

$$\frac{dT_a}{dx} = \sum_i \left[\frac{N_i h_{fg,i} A_{s,i} h_{m,i}\rho_a(X_{s,i}-X)}{C_{p,av}uU_{x,i}} - \frac{N_i h_i A_{s,i}(T_a - T_{d,i})}{C_{p,av}\rho_a u U_{x,i}}\right]$$

$$+\sum_j \left[\frac{N_{b,j}h_{fgb,j}A_{s,i}h_{mb,j}(X_{sb,j}-X)}{C_{p,av}U_{x,j}u} - \frac{N_{b,j}h_{b,j}A_{sb,j}(T_a - T_{db,j})}{C_{p,av}\rho_a U_{x,j}u}\right]$$

$$-\frac{h_a}{C_{p,av}}\left[\frac{1}{u}\frac{du}{dx} + \frac{1}{\rho_a}\frac{d\rho_a}{dx}\right] - \frac{h_{fg,0}}{C_{p,av}}\frac{dX}{dx}$$

$$-\frac{1}{C_{p,av}\rho_a uA}[h_{fg,wall}Ph_{m,wall}\rho_a(X_{wall}-X)$$

$$-h_{wall}P(T_a - T_{wall})]. \quad (8)$$

Conservation of energy for forward and backward moving drops are similar to those used in parallel flow configuration [1].

2.4. *Heat and mass transfer correlations*

The correlations for drag coefficient, mass concentration properties, heat and mass transfer coefficients are same as described in Kachhwaha *et al.* [1] for horizontal parallel flow configuration. The only difference is that Reynolds number of drops in forward flow is based on the following relative velocity represented by equation (7).

2.5. *Effect of drift eliminator*

The evaluation of heat and mass transfer in the drift eliminator is similar to that in horizontal parallel flow configuration model discussed in Kachhwaha *et al.* [1].

2.6. *Boundary conditions*

The detailed boundary conditions used as model input are similar to those used in parallel flow configuration [1].

2.7. *Simulation procedures*

In horizontal parallel flow, spray and air flow are in the same direction, and numerical solution starts from $x = 0$ (spray sheet break-up plane) and marches in the air flow direction. All the initial conditions required at the origin for marching the solution are known and, therefore, air conditions at any location along the duct length can be determined in an explicit manner. The total number of conservation equations involved in this case were 52 (as mentioned in Section 3.7 by Kachhwaha *et al.* [1].

In horizontal counterflow, the air outlet (duct exit) plane coincides with the spray sheet break-up plane. The nozzle direction is opposite to the air flow direction and in the computations the sheet break-up plane has been taken as the origin, i.e. $x = 0$. Therefore, drops at a location in the duct interact with air which has already been cooled and humidified by drops which have travelled further upstream into the duct.

An explicit marching procedure cannot be applied in this situation and iterations are required. In the present case, air exit conditions are assumed and inlet conditions are calculated by marching the solution which is finally then compared with actual inlet conditions. New exit conditions are then assumed and the procedure repeated until the calculated and actual inlet air conditions agree within specified limits. The total number of conservation equations in this case would also be same as in horizontal parallel flow provided all categories of drops have forward motion from the origin and hit the duct wall somewhere downstream of the spray.

In actual practice, an additional complication arises in these procedures due to reversal of drop motion. Depending upon drop diameter and initial velocity, flow reversal takes place at different locations downstream of the spray. These backward moving drops also have two-dimensional motion along the direction of air flow. Some of the relatively larger diameter backward moving drops hit the wall either due to y-direction velocity or gravity and the remaining smaller diameter backward flowing drops reach the origin. All these backward flowing drops contribute significant additional evaporative cooling during their motion in the duct. To incorporate this aspect into the numerical procedure, additional conservation equations for backward moving drops are required. In an extreme case, a possibility exists in which all the forward moving drops have backward motion. Keeping this possibility as a generalized case, these backward moving drops have the same number of conservation equations as for forward flowing drops. Thus, for two-dimensional horizontal counter flow simulation with five drop size categories, the total number of conservation equations is 102 as compared to 52 equations in horizontal parallel flow. Out of the 102 equations, 50 equations are for backward flowing drops for which initial condition are not known *a priori*. Therefore, in addition to outlet air conditions, 50 values each of location, temperature, velocity and diameter, for backward moving drops need to be assumed. The solution is determined iteratively up to the flow reversal point (zero x-velocity component) and compared with calculated values for the forward flowing cases at the same location. Based on the deviation, iterations are performed. The large number of guess values for horizontal counterflow configuration at the beginning of the numerical simulation causes severe convergence problems. This complexity was removed partly by dividing the duct into two halves, upper and lower. Simulations for each half were carried out independently. Thus, the total number of conservation equations for each half are 52 for five drop categories, and the number of guess values are also reduced by half. This step is justified by the fact that drops originating in one half generally do not move into the other half. Further details on this aspect are given in Kachhwaha [2].

In each half of the duct for each backward flowing drop category at the origin plane, five guess values are required, namely diameter, temperature, x- and y-velocities, and y-location. It was observed that convergence is almost impossible if any of the guess values happen to be significantly different from actual value. Such a situation occurs because changes in these values during marching of solution are highly coupled with each other. Hence, a technique was developed so that guess values are in the vicinity of the solution.

The initial conditions for back flow drops are generated in a separate procedure which solves a set of 30 differential equations, namely five equations each for drop mass and energy, 10 equations for drop momentum and 10 equations for trajectory location of drops in x–y plane. These equations (shown in Table 1) are solved in the time domain starting from $t = 0$ at the nozzle outlet and the path of the drops as they travel forward and after loosing momentum start travelling back is traced. The total time domain was kept quite large so that either the drops hit the duct walls or after losing momentum to air, they have reached the plane of the spray sheet break-up due to reversal of motion. In addition to this, the other possibility is that backward moving drops hit the wall before reaching the break-up plane under the influence of the y-component of their velocity. These categories of drops are also considered in backward flow computation. Thus, the results obtained by this procedure at sheet break-up cross-section are, number of categories of backward flowing drops and their diameters, temperatures, x- and y-direction velocities, and y-location. These data have been considered as initial guess values for the main program. While solving these set of equations, the air temperature and relative humidity were kept constant and the equal to the average value of assumed final air condition and inlet air conditions. Due to low evaporative nature of the spray, variation in drop diameter is also very small. Therefore, guess values of velocities for backward moving drops obtained by this procedure are quite accurate. Iterations were, therefore, not necessary for estimating drop velocities and positions.

The final scheme for solving 52 conservation equations is summarized below:

(i) Assume outlet air condition at spray sheet break-up.
(ii) Determine drop size and velocity distribution as explained in Section 4.1, Kachhwaha *et al.*[1].
(iii) Determine number of categories of backward flowing drops and their other conditions needed as initial guess values for the main set of equations using procedure described above.
(iv) Solve the 52 conservation equations in x-direction up to the beginning of duct, and check the various compatibility conditions, i.e. predicted values of air properties with experimentally measured inlet air conditions; and the predicted values of diameter and temperature of backward moving drops with the corresponding values for

Table 1. Equations used for estimation of initial guess values of backward moving drops

Equations for drops	Total number of equations
Conservation of mass	
$\frac{dD_i}{dt} = \frac{-2h_{m,i}\rho_a(X_{s,i}-X)}{\rho_l}$	5
Conservation of momentum	
(a) x-direction	
$\frac{dU_{x,i}}{dt} = \frac{3C_{d,i}\rho_a W_i(U_{x,i}+u)}{\rho_l D_i} - \frac{3U_{x,i}}{D_i}\frac{dD_i}{dt}$	5
(b) y-direction	
$\frac{dU_{y,i}}{dt} = \frac{g(\rho_l-\rho_a)}{\rho_l} - \frac{3}{4}\frac{C_{D,i}\rho_a W_i U_{y,i}}{\rho_l D_i} - \frac{3U_{y,i}}{D_i}\frac{dD_i}{dt}$	5
Conservation of energy	
$\frac{dT_{d,i}}{dt} = \left[\frac{6h_i(T_d-T_{d,i})}{D_i\rho_l} - \frac{6h_{fg,i}h_{m,i}\rho_a(X_{s,i}-X)}{\rho_l D_i}\right]\frac{1}{C_{pd,i}} - \frac{3h_{d,i}}{C_{pd,i}D_i}\frac{dD_i}{dt}$	5
x-direction	
$\frac{dx_i}{dt} = U_{x,i}$	5
y-direction	
$\frac{dy_i}{dt} = U_{y,i}$	5

these drops at the point of reversal of motion as predicted by the equations governing their forward motion.

(v) Change the initial conditions according to error values and repeat the procedure until the convergence criteria are satisfied.

(vi) Repeat the procedure for lower half of the duct.

(vii) Average of DBT and humidity ratio of air in the upper and lower half represents the average values for the duct as a whole.

From spray break-up cross-section to the plane of the drift eliminator, the backward flowing drops are moving in the direction of air and to incorporate the cooling taking place in this region, the parallel flow model is used. The effect of drift eliminator is also taken into consideration.

3. EXPERIMENTAL SET-UP

The experiments were conducted in two phases, i.e. for characterizing the spray and for studying heat and mass transfer in the wind tunnel. Nozzles of outlet diameter 3.2 and 4.8 mm were used in each case separately. Spray characterization was performed in still air, details of which are given in Section 4.1 of Kachhwaha *et al.* [1]. The same wind tunnel was used for counter flow studies. Here, the nozzle was located facing upstream at the centre of exit plane of the wind tunnel (Fig. 2). With the change, the experiments were performed by following the procedure given in Kachhwaha *et al.* [1].

4. RESULTS AND DISCUSSION

4.1. *Experimental results*

The experimental data of counter flow configuration are presented in the Fig. 3. As expected, DBT and humidity ratio changes increase with increasing nozzle pressure at a given air velocity. For constant nozzle pressure, increasing air velocity is generally seen to reduce the magnitude of DBT and humidity ratio changes. These trends are very clearly seen for the 4.8 mm diameter nozzle, where, as explained in Kachhwaha *et al.* [1], water flow rate changes substantially with increasing pressure. The plots also show that DBT changes with 4.8 mm diameter nozzle are significantly greater than those for 3.2 mm diameter nozzle. The same trend is, however, not exhibited in humidity ratio changes. Here too, variations in air inlet conditions and water temperature produces effects which cannot be easily generalized.

4.2. *Simulation results and comparison with experimental data*

During the experiments in counter flow configuration it was noticed that in addition to wet walls of the test-section, the side and bottom walls of the contraction cone upstream of the test section were also wet. This surface area is almost equal to wall area of the test-section. Therefore, simulations have been performed for a duct length of 4 m. The corrected water temperature at the nozzle has been used for the simulations. The data have been split into two parts—one for the upper half of the duct and the other for

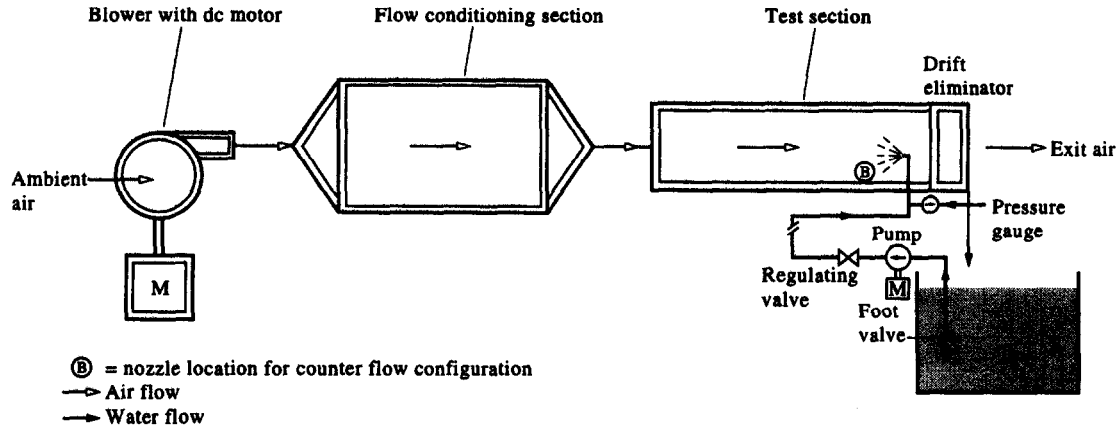

Fig. 2. Schematic diagram of wind tunnel facility.

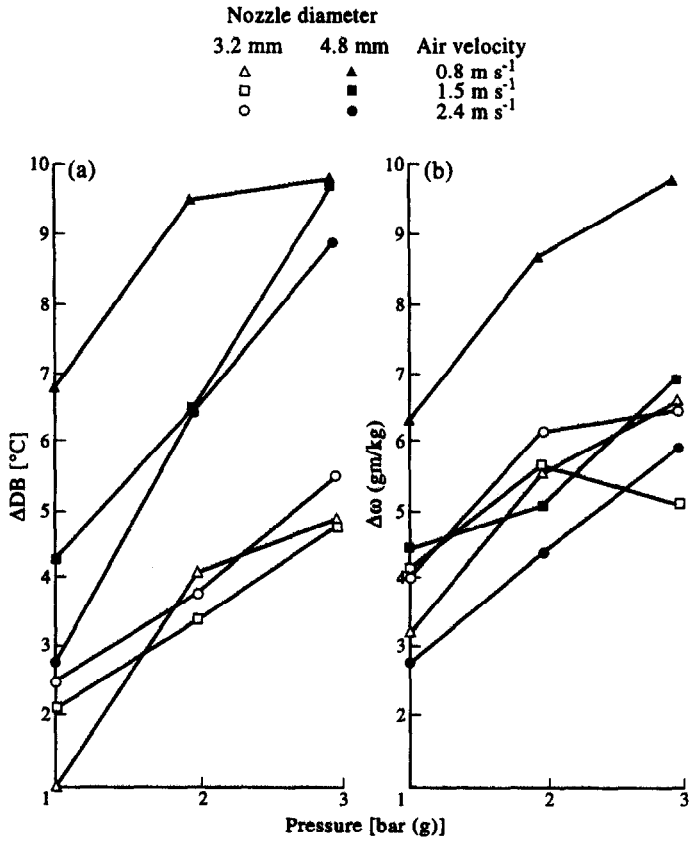

Fig. 3. Change in DBT and humidity ratio with nozzle pressure.

the lower half of the duct. The experimental values of final (outlet) air temperature for upper half of the duct is the mean of the top and centre row of measurements. Similarly, the mean of the centre and lower rows of measurements is taken as the value for the lower half of the duct. The mean of all nine readings have been taken as average values.

Two sets of computations were performed, one for drops injected into the upper half and moving through it and another for drops injected into the lower half and travelling in it. The number of drops injected into the upper half and travelling into the lower half was negligible and, hence, no cross-calculations were necessary. The average of these predictions was taken as prediction for the entire duct.

As in the case of horizontal parallel flow, here also, the predictions using actual drop size were consistently less than measured values. Increasing the

mean drop diameter by 15% and then 30%, resulted in even further underprediction. The optimal match was obtained with 15% reduction in drop diameter. Drop diameter reduction by 30% resulted in a slight overprediction.

Graphic comparisons of average change in DBT and humidity ratio for 3.2 mm diameter nozzle are also shown in Figs 4(a) and (b), respectively. The corresponding data for 4.8 mm diameter nozzle are shown in Figs 5(a) and (b). In all these cases, most of the predictions using 15% smaller diameter agree with experimental data within $\pm 30\%$ where as predictions using actual drop diameter are mostly below zero deviation line.

The average predictions made above are the mean of the predicted values for upper and lower halves. As discussed above, division was made to simplify the computations. However, this also enables us to understand the impact of gravity on the air–water spray interaction. Thus data for the upper half of the duct are shown in Figs 6(a) and (b) for the 3.2 mm diameter nozzle. Both DBT and humidity ratio changes are overpredicted by simulations with drop diameter 15% less than the measured mean diameter. For the 4.8 mm diameter nozzle, predictions are more evenly distributed in the DBT change, Fig 7(a), and that for humidity ratio change match with experimental data within $\pm 15\%$, Fig. 7(b).

For the lower half of the duct with 3.2 mm diameter nozzle, the model underpredicts changes in DBT and humidity ratio changes, Figs 8(a) and (b), respectively, when drop diameter is 15% less than the measured mean value. Similar trends of underprediction are seen in Fig. 9(a) and (b) for 4.8 mm diameter nozzle.

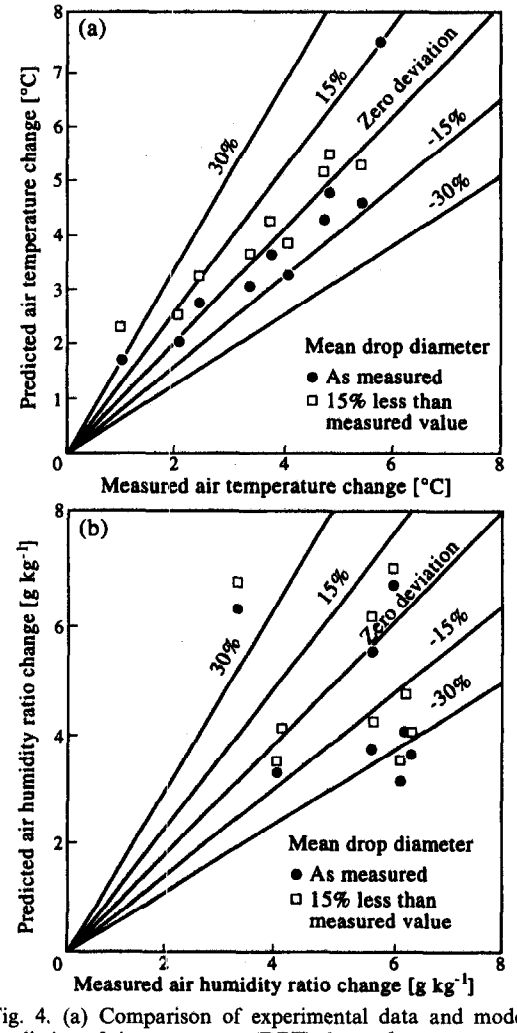

Fig. 4. (a) Comparison of experimental data and model prediction of air temperature (DBT) change for average conditions of the duct (nozzle diameter 3.2 mm); (b) comparison of experimental data and model prediction of air humidity ratio change for average conditions of the duct (nozzle diameter 3.2 mm).

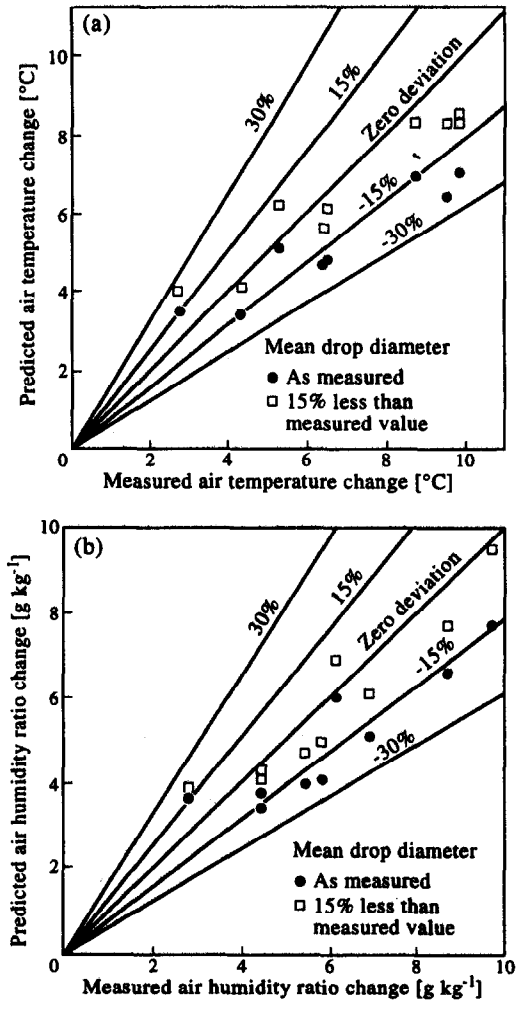

Fig. 5. (a) Comparison of experimental data and model prediction of air temperature (DBT) change for average conditions of the duct (nozzle diameter 4.8 mm); (b) comparison of experimental data and model prediction of air humidity ratio change for average conditions of the duct (nozzle diameter 4.8 mm).

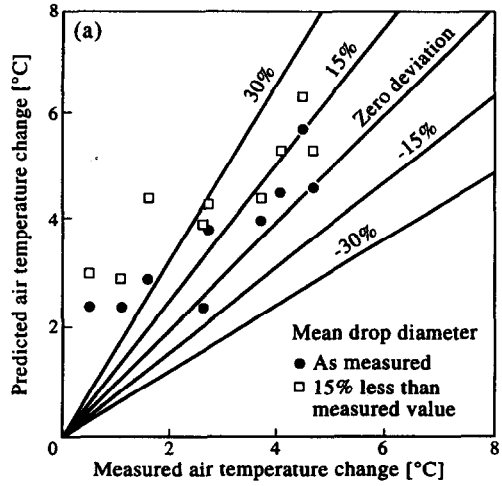

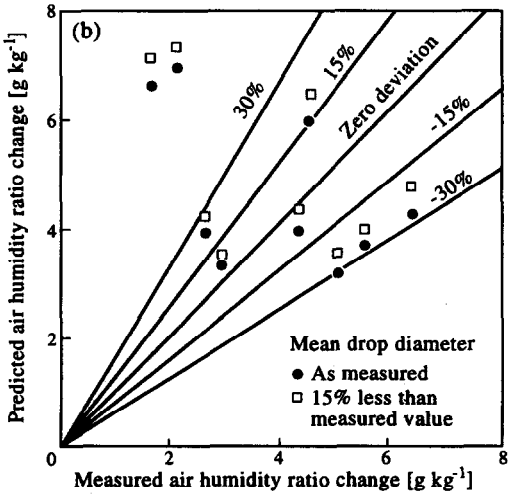

Fig. 6. (a) Comparison of experimental data and model prediction of air temperature (DBT) change for upper half air conditions of the duct (nozzle diameter 3.2 mm); (b) comparison of experimental data and model prediction of air humidity ratio change for upper half air conditions of the duct (nozzle diameter 3.2 mm).

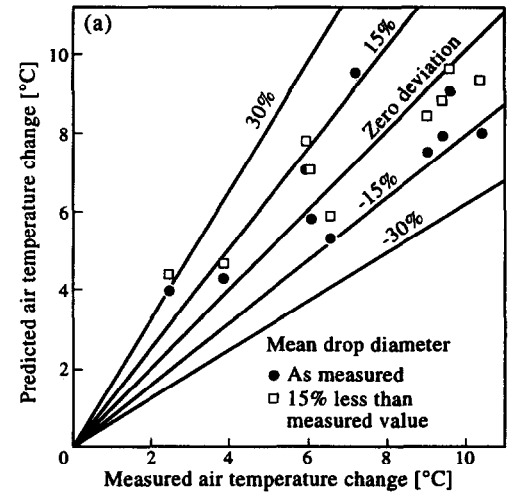

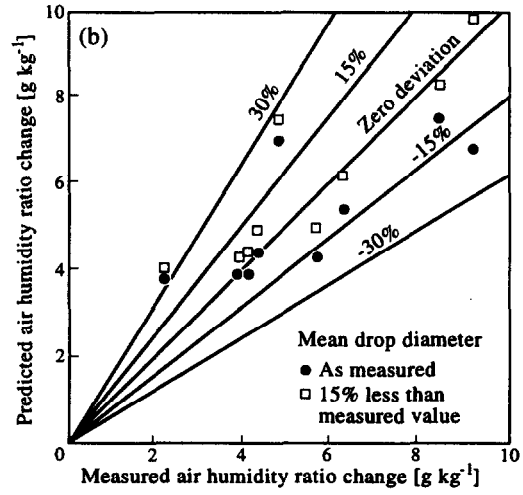

Fig. 7. (a) Comparison of experimental data and model prediction of air temperature (DBT) change for upper half air conditions of the duct (nozzle diameter 4.8 mm); (b) comparison of experimental data and model prediction of air humidity ratio change for upper half air conditions of the duct (nozzle diameter 4.8 mm).

These sets of predictions indicate an overprediction trend from the duct upper half but an underprediction trend for the duct lower half. The reasons for this behaviour can be seen in Figs 10 and 11 where drop trajectories and air condition variation based on 15% decrease in drop diameter for a typical case [nozzle diameter 4.8 mm, pressure 2 bar (g)] are shown. The difference between lower and upper half trajectories is in the 174 μm diameter drops which interact with air for a longer period in the upper half than in the lower half. Besides this effect, due to the effect of gravity, residence time for lower half trajectories is relatively smaller as compared to the upper half. Due to these reasons, there is 0.5°C underprediction in upper half as compared to bottom half. Between the break-up plane and drift eliminator inlet there is a gap of 0.2 m. In the upper half of the gap, drops of diameter 58 and 174 μm exit the duct with a velocity slightly less than the air velocity. The total number fraction of 174 μm drops is around 50% which causes an additional evaporative cooling of around 1°C (see Fig. 10). In the bottom half, only 58 μm diameter drops exit (5% number fraction) which contributes only 0.1°C evaporative cooling in the bottom half. The effect of drift-eliminator is common to both halves. This argument also explains the variation of humidity ratio in the two halves. Further, in the wind tunnel, some drops upon drifting with the air in the upper half fall downwards due to gravity and contribute towards cooling in the lower half. Thus, experimentally, the lower half exhibits greater cooling than the upper half, in the case of 3.2 mm diameter nozzle. A similar trend is not so clearly discernable for the 4.8 mm diameter nozzle. This difference may be attributed to the relatively greater cone angle in 4.8 mm diameter nozzle as compared to the 3.2 mm diameter nozzle. In the case

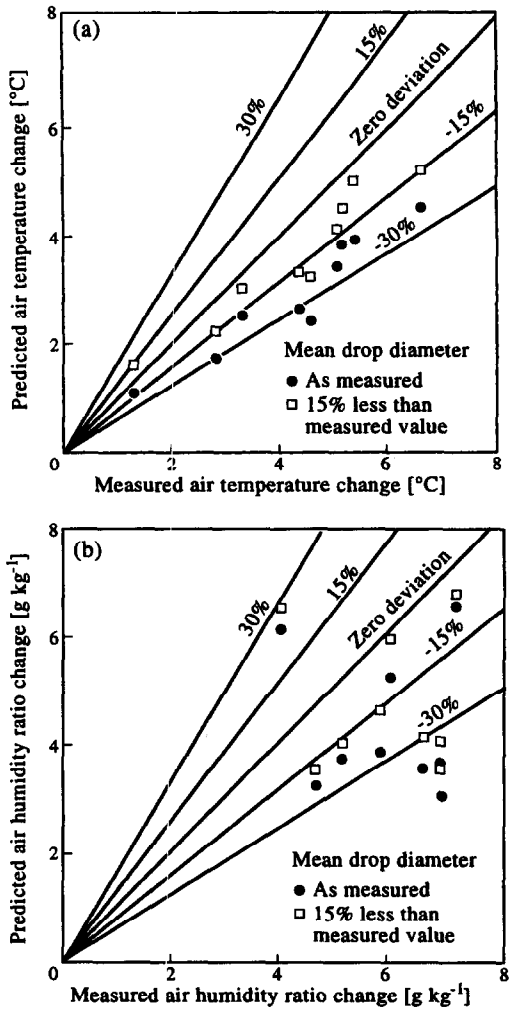

Fig. 8. (a) Comparison of experimental data and model prediction of air temperature (DBT) change for lower half air conditions of the duct (nozzle diameter 3.2 mm); (b) comparison of experimental data and model prediction of air humidity ratio change for lower half air conditions of the duct (nozzle diameter 3.2 mm).

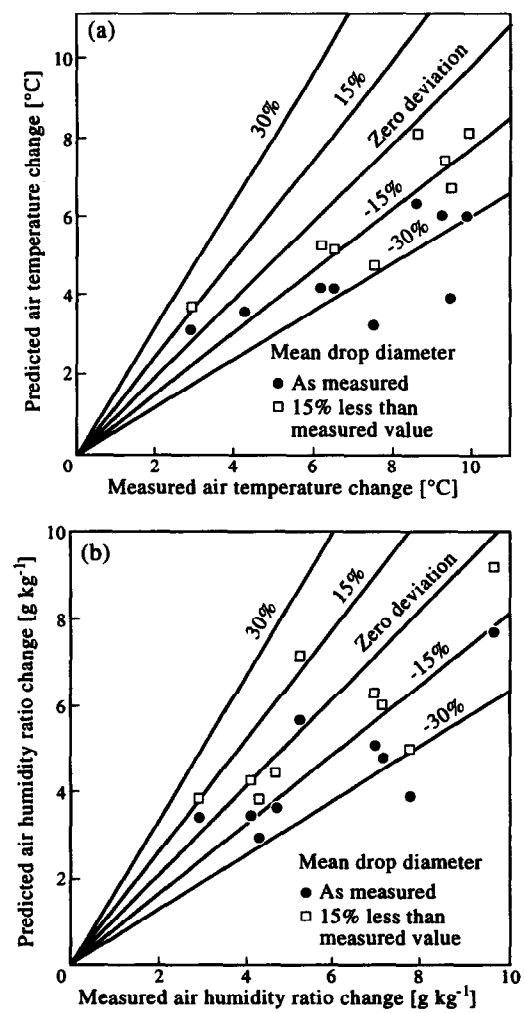

Fig. 9. (a) Comparison of experimental data and model prediction of air temperature (DBT) change for lower half air conditions of the duct (nozzle diameter 4.8 mm); (b) comparison of experimental data and model prediction of air humidity ratio change for lower half air conditions of the duct (nozzle diameter 4.8 mm).

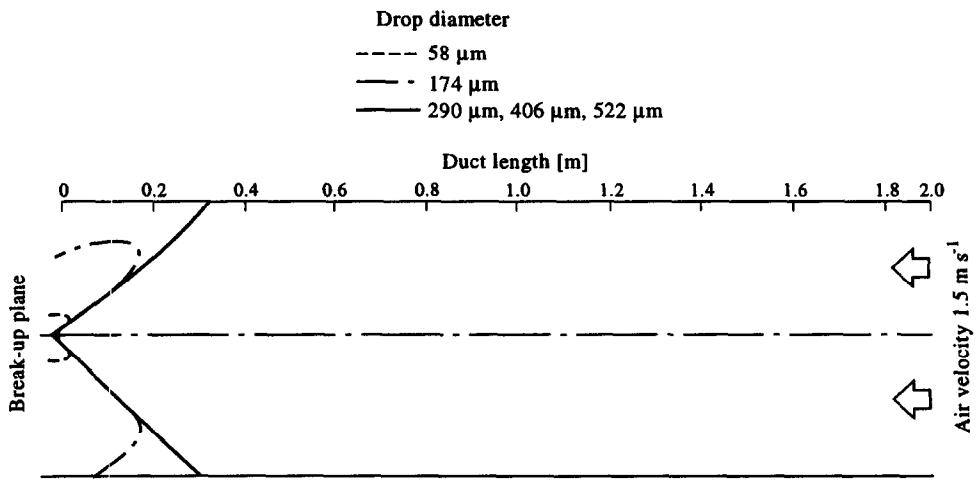

Fig. 10. Drop trajectories in the duct [nozzle diameter 4.8 mm, pressure 2.0 bar (g)].

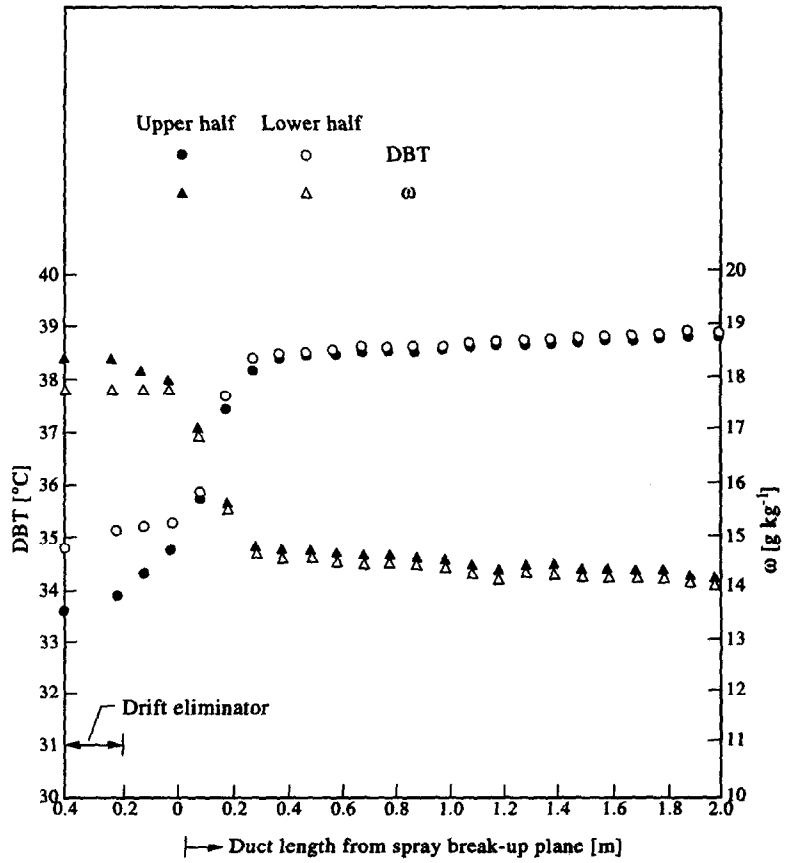

Fig. 11. DBT and humidity ratio variations along the duct for horizontal counter flow [nozzle diameter 4.8 mm, pressure 2 bar (g)].

of greater cone angle, back flowing drops are more uniformly spread in the ducts with the result that their contribution to cooling in the two halves is almost equal. With low cone angles, drops in the upper half travel longer distances upon drifting and have a tendency to come down to the lower half of the duct rather quickly. For this reason greater cooling is expected in the lower half. Similar trends are observed in humidity ratio changes.

In the simulations, the trajectories of all drops are taken to be in the vertical centre plane of the duct. This modelling feature treats drop trajectories at non-vertical azimuthal angles in the same manner as if they were originating in the vertical plane. As a result, the modelled trajectories are smaller in length than those in reality. For instance, a drop whose motion at sheet break-up is at 45° to the horizontal, either upwards or downwards have to travel a longer distance to approach the duct wall as compared to a drop whose motion at break-up is only in a vertical plane. The model, is, therefore, likely to underpredict the cooling extent, a trend clearly seen in Figs 4 and 5.

5. CONCLUSION

The main objective of the research work was to develop a simple and efficient numerical model for estimation of heat and mass transfer between water spray drops and air stream in horizontal counterflow configuration to enable accurate prediction of evaporative cooling performance. The predictions are within $\pm 30\%$.

REFERENCES

1. Kachhwaha, S. S., Dhar, P. L. and Kale, S. R., Experimental studies and numerical simulation of evaporative cooling of air with a water spray: part I—horizontal parallel flow. *International Journal of Heat and Mass Transfer*, 1996a (submitted).
2. Kachhwaha, S. S., Some studies on spray type evaporative cooling process. Ph. D. thesis, Mechanical Engineering Department, IIT, Delhi, 1996.